

Segmented variations in tectonic geomorphology of Datong-yangyuan fault zone, NW Beijing, China

Cheng Shaoping and Yang Guizhi

Institute of Geology, State Seismological Bureau, Beijing 100029, China.

(Received 15 November 1997; accepted 22 January 1998)

Abstract: *The Datong-Yangyuan fault zone (DYFZ) is the largest normal fault in the late Cainozoic Shanxi rift system. Heights of late-Quaternary fault scarps and their along-trending distribution pattern divide the fault zone into two segments, the southwestern segment (SWs) and the northeastern segment (NEs). Between these two segments there are significant variations in mountain front and piedmont slope tectonic geomorphology, mountain front sinuosity, valley width-depth relief ratio and stream gradient index, as well as in the sequence of the micro-physiographic stages, erosion - aggradation - erosion along the NEs and aggradation-erosion-aggradation along the SWs. Rate of faulting and downcutting, fault behaviour and segment boundary characteristics seem to be responsible for such contrast in tectonic geomorphology of the two segments of the fault zone. The boundary between the two segments is characterised by a fault overlap zone, along which a fault displacement deficit has occurred. Therefore, fault behaviour and the distribution of overlapping faults are conjointly responsible for the variations in geomorphology of the Datong-Yangyuan fault zone.*

Key Words: *Segmentation, Tectonic Geomorphology, Datong-Yangyuan Fault Zone, Shanxi Rift System, China.*

INTRODUCTION

SEGMENTATION

The Datong-Yangyuan fault zone (DYFZ) is the largest normal fault in the late Cainozoic Shanxi rift system (Xu *et al.*, 1996). It runs along the southern margin of the Datong-Yangyuan Basin at the northern end of the rift system, with a total length of 140 km and a SW-NE strike (Fig. 1). The basement rocks exposed along the fault zone consist of Archaean gneiss or metaconglomerate, and Proterozoic and Paleozoic limestone, as well as a few Mesozoic magmatic rocks and Quaternary basalt. The segmentary development of normal faults plays an important role in evolution of fault zones (Mandl, 1988; Crone and Heller, 1991; Stewart and Hancock, 1991). Studies on the late Cainozoic volcanic rocks and Pleistocene lacustrine deposits associated with the rifting have greatly advanced in recent years (Chen *et al.*, 1992; Xia, 1992), but little attention has been drawn to the post-volcanic or post-lake sections, especially the late Pleistocene fault movement of the DYFZ. Based on the relationships between tectonics and morphology, this paper demonstrates the segmented variations in tectonic geomorphology. It also discusses possible causes for these variations.

Late-Quaternary Fault Scarps

The late Quaternary fault scarps are almost continuously distributed along the DYFZ. They are usually developed in late-Quaternary loessal soil and sandy gravel deposits. In places they are formed in the basement rocks exposing a fracture zone of several tens of meters wide and many fault surfaces.

A 230000 a old basalt (Chen *et al.*, 1992) at Qiulin in the central part of the fault can provide a time of formation for the fault scarp. Measurements of the basalt weathering-rind taken from the strath of the Qiulin stream across the fault scarp average 2.26-3.00 mm, from which an age of 122800 a can be calculated according to the weathering-rind thickness curve of the northernmost China (Cheng *et al.*, 1991a). This age indicates the separation of the strath from water followed immediately by weathering. The offset of the basalt will have occurred after this age.

Segmentation

Based on height of the late-Quaternary fault scarp

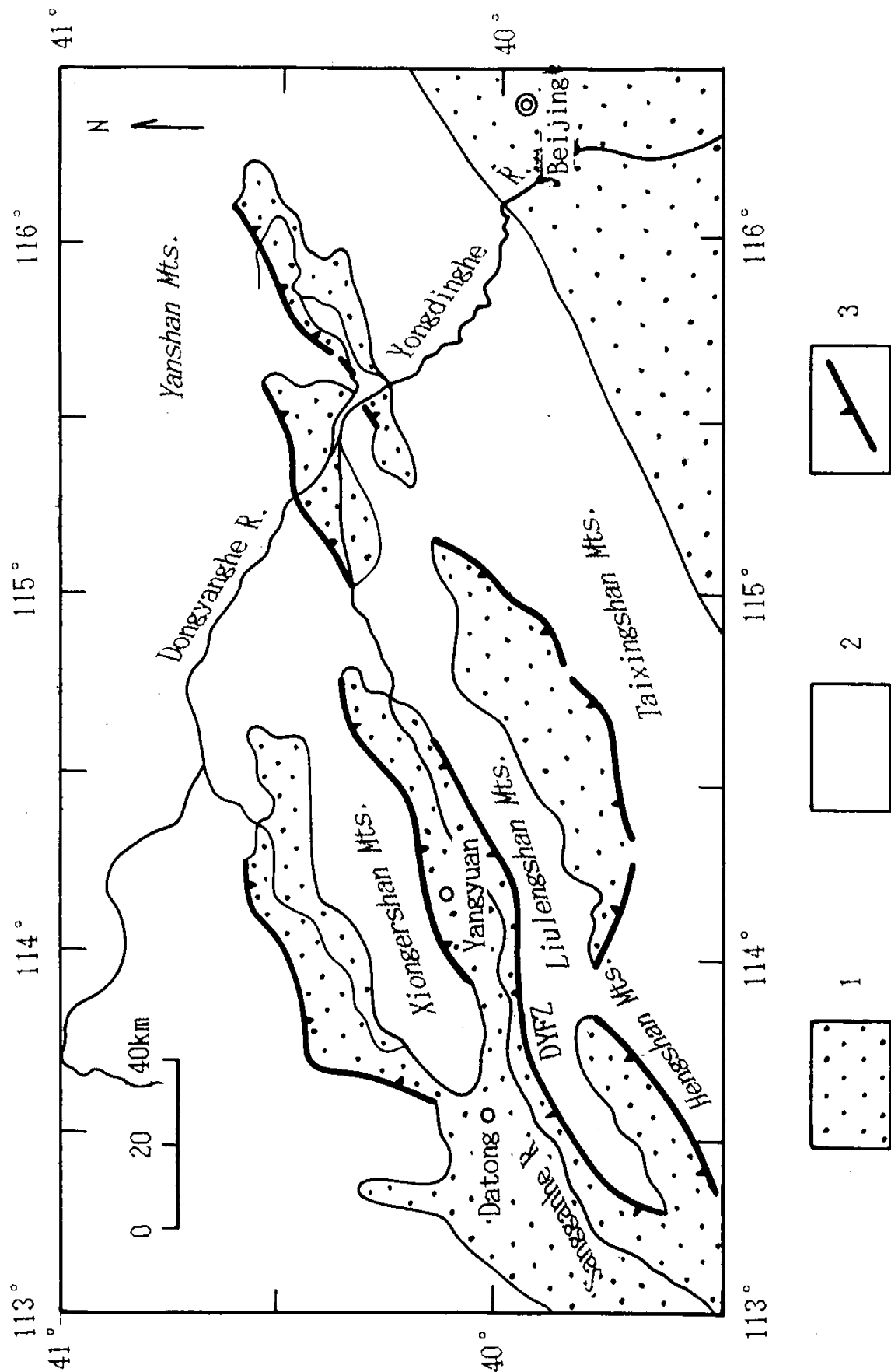


FIG. 1. Simplified tectonic map of the northeastern tip of the Shanxi rift system, showing the distribution of basins (1), ranges (2) and faults (3).

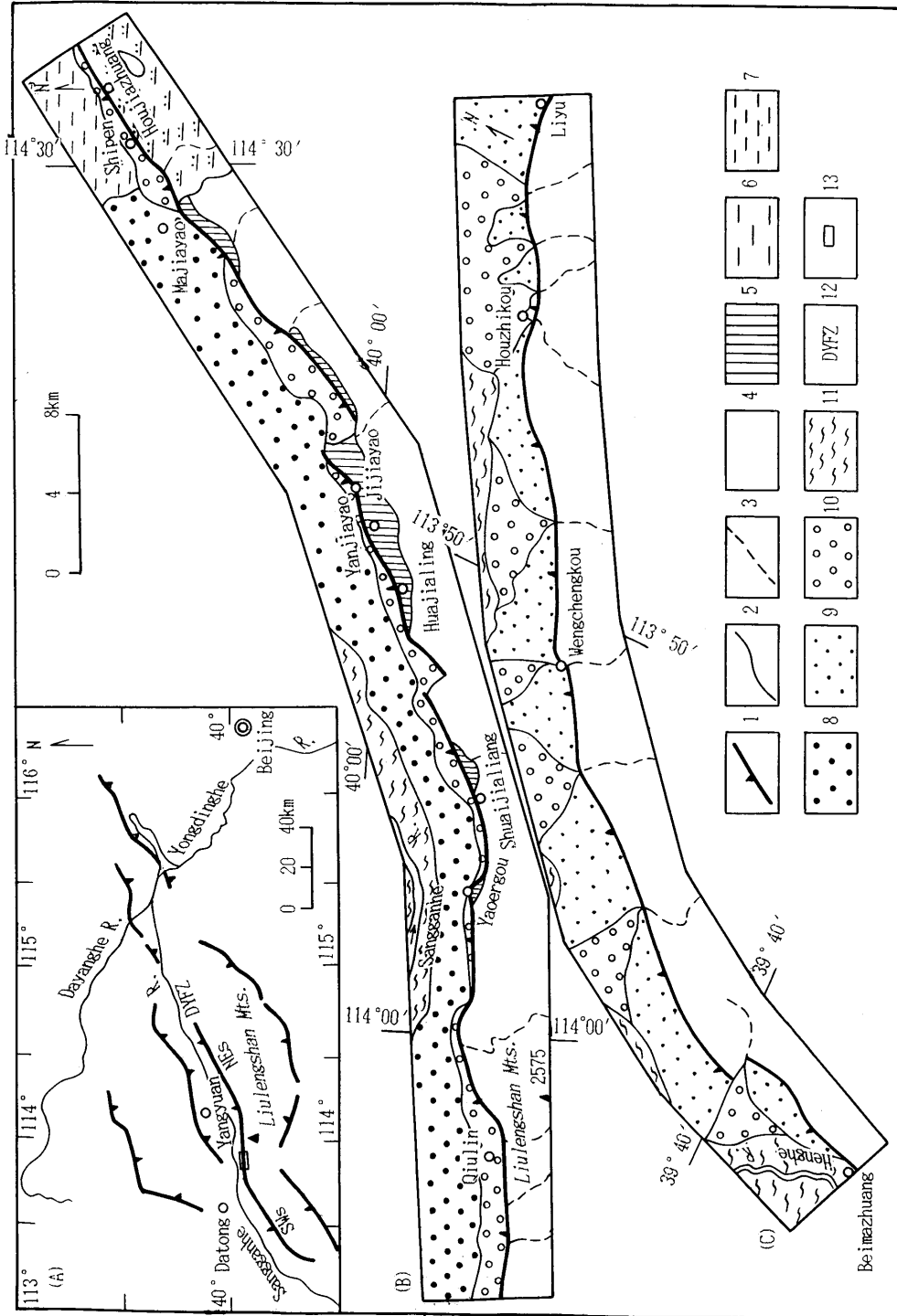


FIG. 2. Map of tectonic geomorphology of the DYFZ, showing (A) the location of the fault zone, (B) tectonic geomorphology of the northeastern segment (NEs) and (C) tectonic geomorphology of the southwestern segment (SWs). Note that B and C are not consecutive and there is segment boundary area between them as shown in Figure 11a. (1) fault, (2) geomorphological unit boundary, (3) stream, (4) mountains, (5) uplifted pediment, (6) uplifted lacustrine plain, (7) present lacustrine plain, (8) A_1 (Q_1^1) alluvial fan, (9) A_2 (Q_2^2) alluvial fan, (10) A_3 ($Q_3^2 + Q_4^1$) alluvial fan, (11) present flood plain, (12) Datong-Yangyuan fault zone, (13) Figure 11a area.

and their along strike distribution pattern, the fault can be divided into two discrete segments: the southwestern segment (SWs) and the northeastern segment (NEs) (Fig. 2). For each segment, the fault scarp is relatively higher in its central part and significantly decreases towards both its tips. Moreover, there is a greater difference in fault scarp height between the two segments, with generally much higher fault scarps on the NWs than on the NEs (Fig. 3a).

The topography of crests on the footwall reflects the long-term slip history of the fault zone. A topographic profile made parallel to, and 2km south of it, indicates that there is a good consistency between the crest relief and the late-Quaternary fault scarp distribution (Fig. 3b and a), supporting the segmentation in fault scarp height.

The parameters of the late-Quaternary segmentation for the DYFZ are shown in Table 1.

MOUNTAIN FRONT

Implication of Geomorphological Indices

A mountain front generated by faulting is a zone on which fluvial systems can adjust themselves to local base-level processes. Such relative adjustment can be examined by the morphometrical analysis which include several useful geomorphological indices such as mountain front sinuosity (S) and valley width-depth relief ratio (V_f) (Bull and McFadden, 1977), as well as stream-gradient index (K) (Hack, 1973).

Mountain front sinuosity (S) can indicate a relationship between faulting (in order to maintain a straight mountain front) and erosion (in order to make a mountain front sinuous). A very straight mountain

front on which active faulting is dominant over erosion has an S value close to 1.00, whereas a relatively sinuous mountain front on which basal erosion and sedimentation play a more important role has a significantly larger S value.

Valley width-depth relief ratio (V_f) reflects the adjustment between channel downcutting and lateral erosion, under which V-type canyons or valleys with wider floors appear on the mountain front. Reaches with lower V_f values are controlled by channel downcutting due to local base level falling. In contrast, reaches with higher V_f values are dominated by lateral planation.

Stream-gradient index (K) is closely associated with fault displacement increments on mountain fronts. Streams with larger displacement increments have higher K values on their outlets on mountain fronts, otherwise they have lower (Cheng *et al.*, 1991b).

Variations in Geomorphologic Index

Three geomorphological indices in this study were measured on 1:10000 scale topographic maps and were calculated using Bull and McFadden's (1977) formula for V_f and S and the Hack's formula (1973) for K (Fig. 3 c-e and Table 2).

The distribution of geomorphological indices shows a variation between segments in mountain front tectonic geomorphology. As shown in Figure 3 (c)-(e) and Table 2, there is a large difference in K values but a small difference in S and V_f values between these two segments, indicating firstly that the mountain front tectonic geomorphology for both segments is mainly controlled by faulting rather than fluvial erosion, and secondly, that the NEs is more strongly constrained by faulting than the SWs.

Table 1. Parameters of segmentation.

Segment	Beginning and end	Height of Quaternary (m)	later-fault-scarp	Trending	Segment boundary	Segment length (km)
		Central	End			
Southwestern segment	Beimazhuang-Liyu	30	20-25 (east end) 8-10 (west end)	N 50° - 60° E	_____	61
Northeastern segment	E Dawangcun -Houjiazhuany	30-42	25	N50° - 60° E	Overlapping -faults _____	70

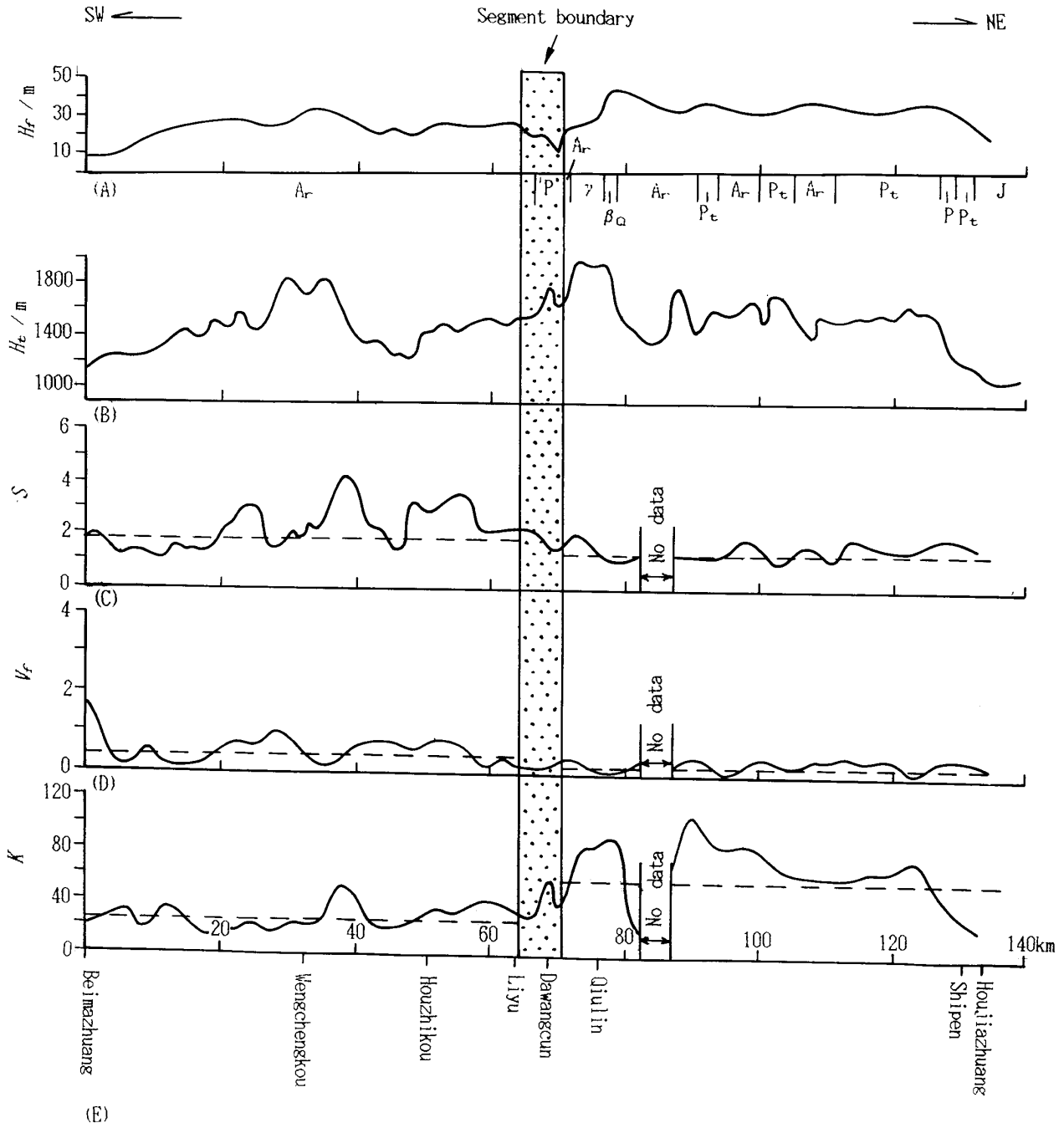


FIG. 3. Distribution of Geomorphological parameters along the fault strike showing segmented contrast in geomorphological parameters between segments. (A) Late-Quaternary fault scarp height (H_f); (B) topographic relief of mountain crests on the footwall (H_t); (C) mountain front sinuosity (S); (D) valley width-depth relief ratio (V_f); (E) stream-gradient index (k); in (C)-(E), solid line represents smoothed curve average and dashed line mean curve. (Ar) metaconglomerate or gneiss, similarly hereinafter; (Pt) dolomitic limestone, (P) Limestone, (J) volcanic rock, (β_Q) basalt, (γ) granite.

Table 2. Values of geomorphological indices.

Fault segment	sample	S			V_f			K		
		Mean	Max	Min	Mean	Max	Min	Mean	Max	Min
SWs	140	1.93	5.15	1.00	0.49	1.88	0.09	27.18	86.25	6.23
NEs	92	1.57	3.2	1.00	0.39	1.60	0.01	56.61	119.08	16.4

PIEDMONT SLOPE

Late-Quaternary Alluvial Fan Deposits

The piedmont slope of the fault zone has alluvial fan deposits, whose lithology, buried sediments, and timing of aggradation show significant difference between both segments.

Early late-Pleistocene (Q_3^1) alluvial fan deposits

For the SWs, a complete Q_3^1 deposit usually consists of an upper layer of loessal soil containing coarse sands and fine gravels and a lower layer of sandy gravels, with a total thickness of 20 m (Fig. 4a). Where the upper loessal soil has been eroded, a 0.4-1.0m thick paleosol remains on the lower sandy gravels (Fig. 4b).

For the NEs, there are significant differences in the Q_3^1 deposit lithology. The western part consists of thick loessal soil interbedded with sandy gravels, overlying on the basement rocks (Fig. 5a), whereas the eastern part consists of very thick loessal soil overlying the lacustrine sediments (Fig. 5b).

The SWs Q_3^1 is almost completely buried by the Q_3^2 deposits, with only a few exposures seen at some stream-banks (Fig. 4b), whereas the NEs Q_3^1 is often covered with the $Q_3^2 + Q_4^1$ deposits towards the upper part of the fan, and exposed towards the lower part of the fan.

In the Datong area the latest basalt magma activity ceased at 98000 a B.P. (Li and Sun, 1984), which approximately represents the initiation of Q_3^1 aggradation on the SWs. The end of aggradation might have been between 98000 a B.P. and 48300 a B.P. when the upper loessal soil started to erode (Fig. 5a).

The Q_3^1 aggradation on the NEs was initiated at 70800 a B.P. (Fig. 6b). A conclusion is that the initiation of the Q_3^1 aggradation on the SWs was earlier than on the NEs.

Late-Pleistocene (Q_3^2) alluvial fan deposits

For the SWs, the Q_3^2 deposits that form alluvial fan A_2 (Q_3^2) are dominantly composed of thick-bedded loessal soil containing thinly bedded and lens-shaped sandy gravels (Fig. 5a), with a few boulders. An aggradation might have been initiated at 48300 a B.P. (Fig. 5a). In contrast with the SWs, the NEs generally lacks Q_3^2 deposits.

Latest late-Quaternary-early Holocene ($Q_3^2 + Q_4^1$) alluvial fan deposits

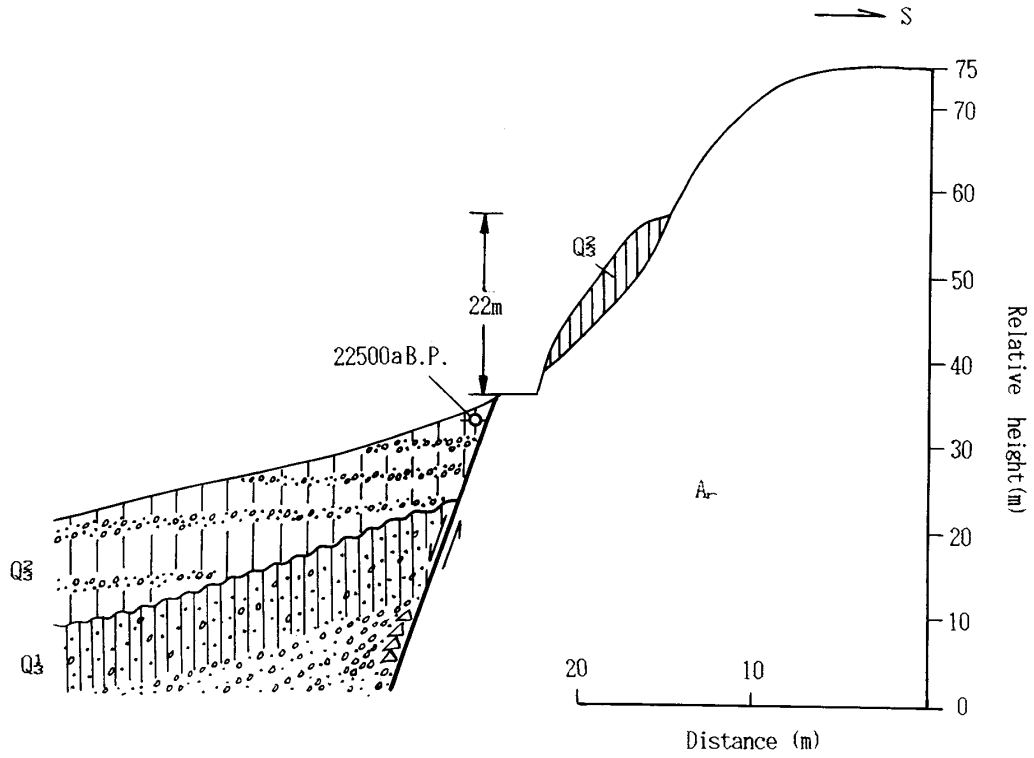
The $Q_3^2 + Q_4^1$ deposits for the SWs are basically well-stratified sands, gravels, and reworked loessal soil, which were primarily deposited by the larger streams shedding from the mountains. For the NEs the sandy gravel deposits are dominantly composed of boulders and pebbles, which usually lack the reworked loessal soils of the SWs. Geomorphologically, the $Q_3^2 + Q_4^1$ deposits consist of alluvial fan units A_3 ($Q_3^2 + Q_4^1$).

The $Q_3^2 + Q_4^1$ deposits for the SWs might have occurred between 27600 a B.P.-5600 a B.P., which are the times of formation of T_3 (Q_3^2) and T_1 (Q_4^1), respectively (Fig. 6a), and for the NEs between 25000 a B.P. at which time the paleosol on the Q_3^2 surface started developing, 3900 a B.P. (Fig. 6b).

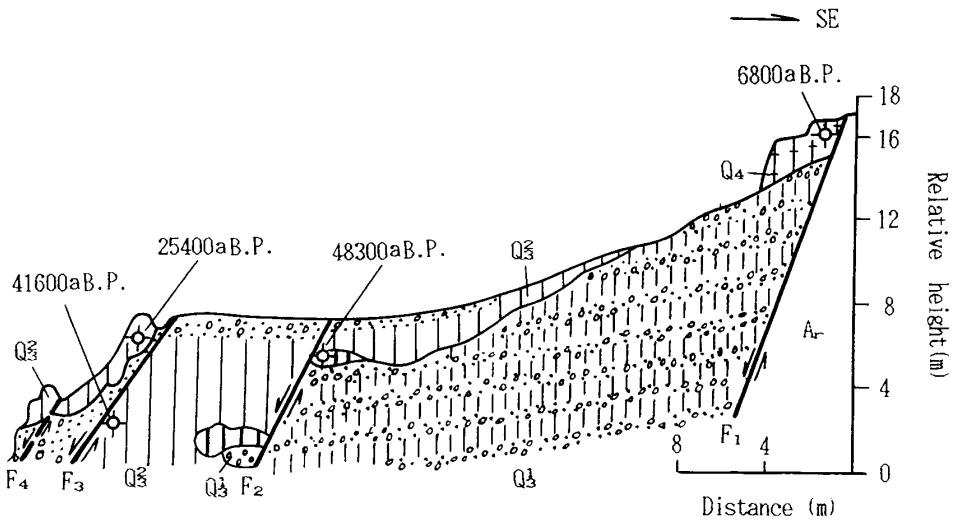
Variations in Mode of Piedmont Slope Warping and the Pattern of Alluvial Fan Assemblages

The SWs

The alluvial fan A_2 (Q_3^2) apexes have a slope up to $10^0 - 14^0$ and an incisional depth of 20-35m. For the alluvial fan A_3 ($Q_3^2 + Q_4^1$), however, the apex slopes are $6^0 - 8^0$. This morphology of the piedmont slope indicates that upwarping occurred at the near-fault part of the A_2 (Q_3^2) alluvial fan (Fig. 7a), creating a landform assemblage of the younger A_3 ($Q_3^2 + Q_4^1$) inset into the older A_2 (Q_3^2) (Fig. 2c).

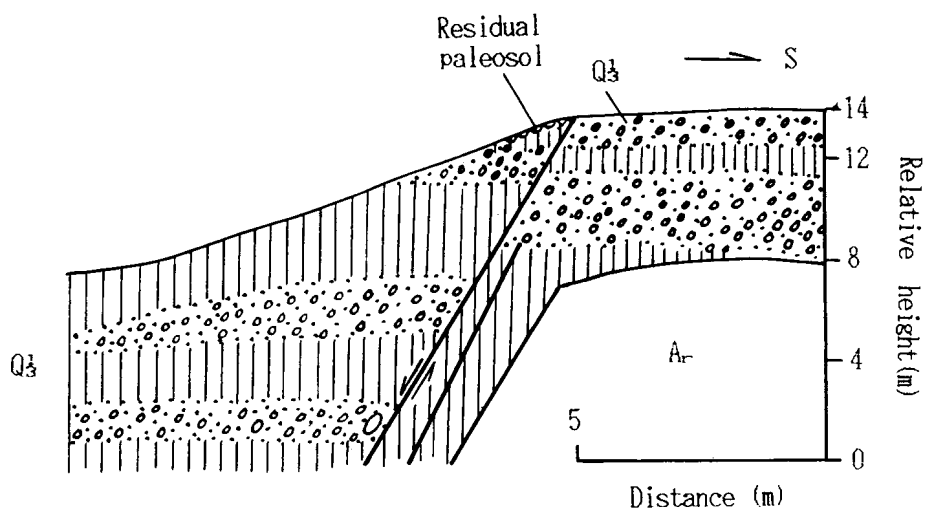


(A)

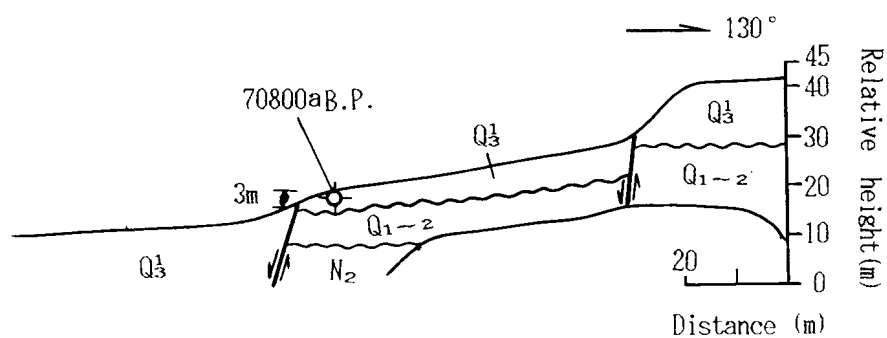


(B)

FIG. 4. Cross-section west of Liyu (A) and Houzhikou (B), showing the lithology of the Late-Quaternary alluvial fan deposits Q_3^1 for the SWs. * Sampling site and age of thermoluminescence dating; Q_3^1 and Q_3^2 . For explanatory notes on lithology see text; Q_4 silty clay.

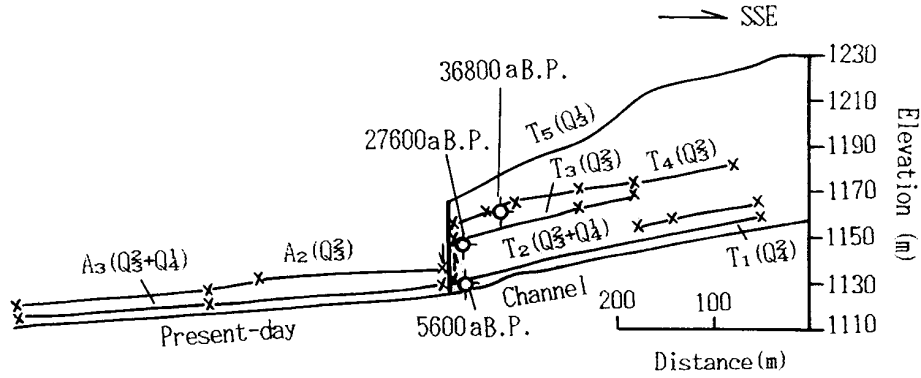


(A)

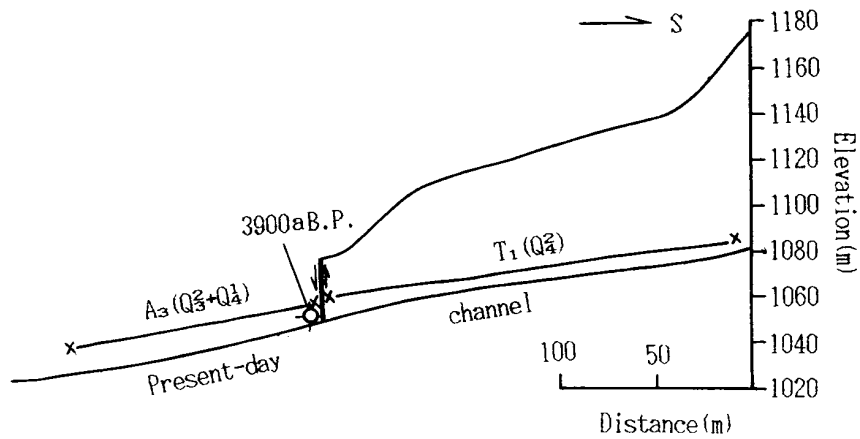


(B)

FIG. 5. Cross-section northeast of Yanjiayao(A), and Shipen(B), showing the lithology of the late Quaternary alluvial fan deposits Q_3^1 for the NEs. N_2 Lateritic gravels; Q_{1-2} Lacustrine sediments; Q_3^1 . For exploratory notes on lithology see text. Geomorphologically, the Q_3^1 deposits form alluvial fan A_1 (Q_3^1).



(A)



(B)

FIG. 6. Terrace-alluvial fan longitudinal profiles along the Wengchengkou Stream (A) and along a stream southeast of Yaoergou (B), showing the initiation timings of the Q_3^2 aggradation and the $Q_3^2 + Q_4^1$ aggradation for the SWs (A) and the end of timings of the $Q_3^2 + Q_4^1$ aggradation for the Nes (B), and also showing level separations between terraces and alluvial fans due to influence of faulting. $T_1(Q_4^1)$ - $T_5(Q_3^1)$ terrace; $A_2(Q_3^2)$ and $A_3(Q_3^2 + Q_4^1)$ alluvial fan; \times measuring site for terraces.

The Nes

In contrast, within the NEs, the A_3 ($Q_3^2 + Q_4^1$) alluvial fans have $6^\circ - 8^\circ$ fan surface slopes and 4-8m incisional depths, however, the distal parts of the A_1 (Q_3^1) alluvial fans have only $2^\circ - 3^\circ$ slopes. This suggests that downwarping might have occurred on the near-fault part of the A_1 (Q_3^1) alluvial fans (Fig. 7b), forming a landform assemblage of the younger A_3 ($Q_3^2 + Q_4^1$) overlapped onto the A_1 (Q_3^1) (Fig. 2b).

UPLIFT PEDIMENT

The uplifted pediment is a landform associated with tectonism within the NEs. It is distributed over a length of about 40 km from Yaoergou to Majiayao, with a width of 750-1400 m.

Lacustrine and Fluvial Covers

On the surface of the pediment, generally, there is a lacustrine gravel and clay layer underlain by a fluvial loessal soil containing pebble (Fig. 8a and b). This indicates that the pediment should have been resulted from abrasion of the ancient lake earlier on, in conjunction with mountain stream erosion. The ancient lake finally settled on the pediment at 111500 a B.P.(Fig. 8b).

Erosional Surface Sequence

The frontal rim of the pediment consists of three erosional surfaces and their scarps that are indicative of alternations of periods of activity and quiescence in tectonism. The scarps represent tectonic activity and erosional surfaces tectonic quiescence. The highest erosional surface (a), the main body of the pediment,

was uplifted by faulting initiated at 111500 a B.P.. The two lower erosional surfaces (b) and (c) are associated with later fault activity. The erosional surface (b) was uplifted at about 43700 a B.P., based on thermoluminescence dating for the surface loessal soil (Deng *et al.*, 1994)(Fig. 8c). Table 3 shows the morphology of the uplifted pediment at several sites.

LATE-QUATERNARY MICRO-PHYSIOGRAPHIC STAGES

Micro-physiographic States of the DYFZ

The differentiation between the late-Quaternary micro-physiographic stages of the fault zone establishes the relations between events, such as faulting, erosion, and aggradation on the mountain front. During aggradation, alluvial fan accumulated whose surface has tended to be graded by the slopes of upstream channels, eliminating fault displacements. An aggradational stage can therefore be associated with a period of little faulting. In contrast, fault movements upset the common gradient between channels and fan surfaces and processes producing erosion can play a dominant role on alluvial fan surfaces. In this way, an erosional stage can be related to a period of active faulting.

Based on data from dating of alluvial fan sediments, terraces, and uplifted erosional surfaces, the micro-physiographic stages were differentiated for both segments, as shown in Table 4.

Variation in Evolutionary History

As shown in Figure 8, prior to 36800 a B.P., the SWs underwent the evolutionary stage of aggradation-erosion-aggradation, whereas the NEs went through the erosional stages of aggradation- erosion with an

Table 3. Morphology of the uplifted pediment.

Site	Erosional surface (a)			Erosional surface (b)		Erosional surface (c)	
	H* (m)	S** (°)	h*** (m)	H (m)	h (m)	H (m)	h (m)
Shuaijia-liang	1040	5.71	20	1020	20(?)		
Huajia-ling	1010	7.26	10	1000	20(?)		
Lijiayao	1010	5.88	10	995	10	985	10
Majiayao	975	7.94	12	963	7	956	7

* Frontal elevation

** Slope

*** Scarp height

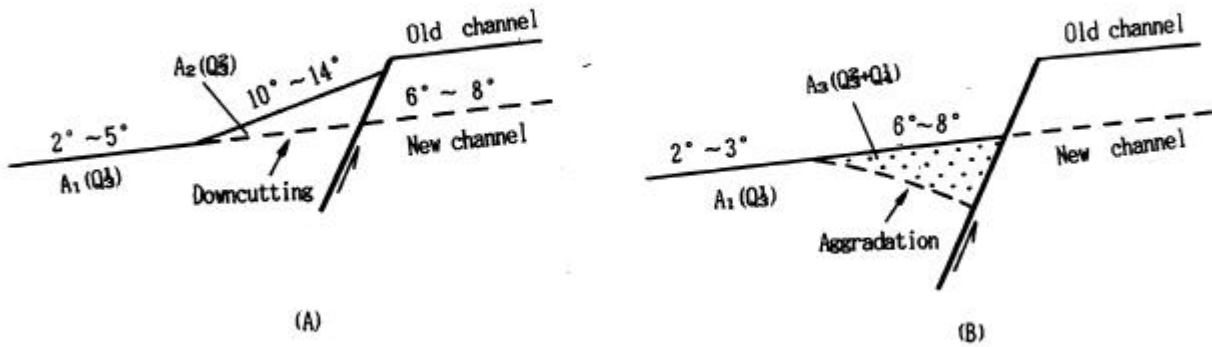


FIG. 7. Different patterns of warping on normal fault piedmont slopes (Modified from Wallace, 1978), showing upwarping of the $A_2(Q_3^2)$ near-fault part for the SWs (A), and downwarping of the $A_1(Q_3^1)$ near-fault part for the NEs (B).

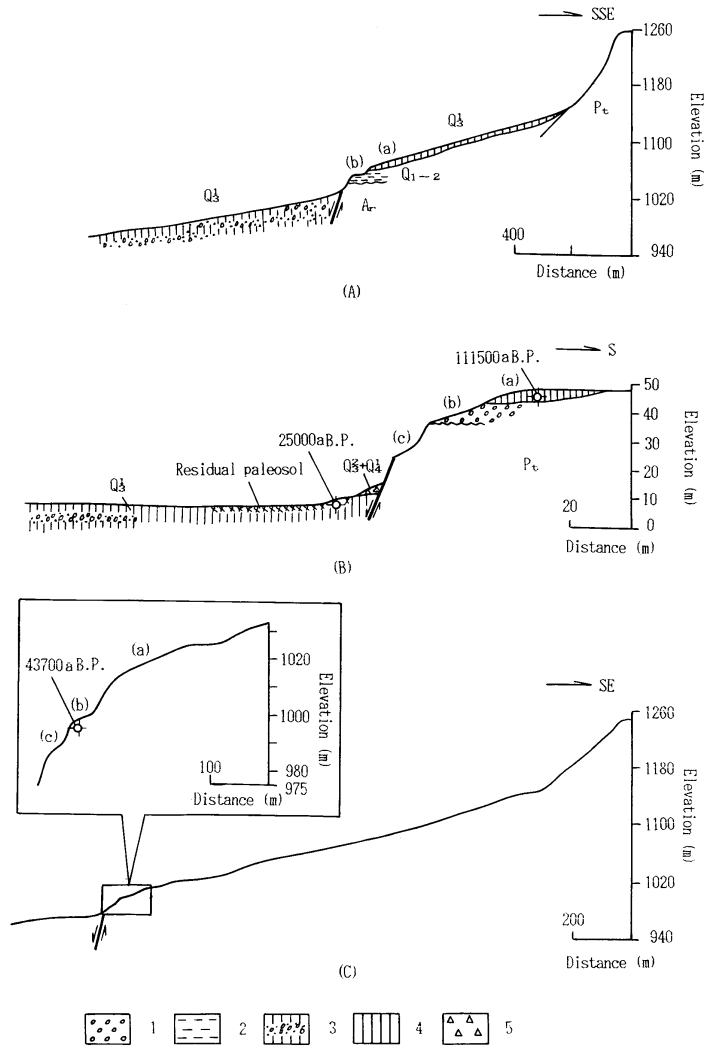


FIG. 8. Geological and topographic profiles of the uplifted pediment of the NEs at Huajialing (A), Majiayao (B), and Jijiayao (C), showing a lacustrine layer overlain by a fluvial layer remains on the surface of the pediment. (a), (b), and (c) represent the erosional surfaces. 1 Lacustrine gravel; 2 Lacustrine clay; 3 Loess containing sandy gravel layer; 4 Loessal soil; 5 Colluvial and/or slope wash clasts.

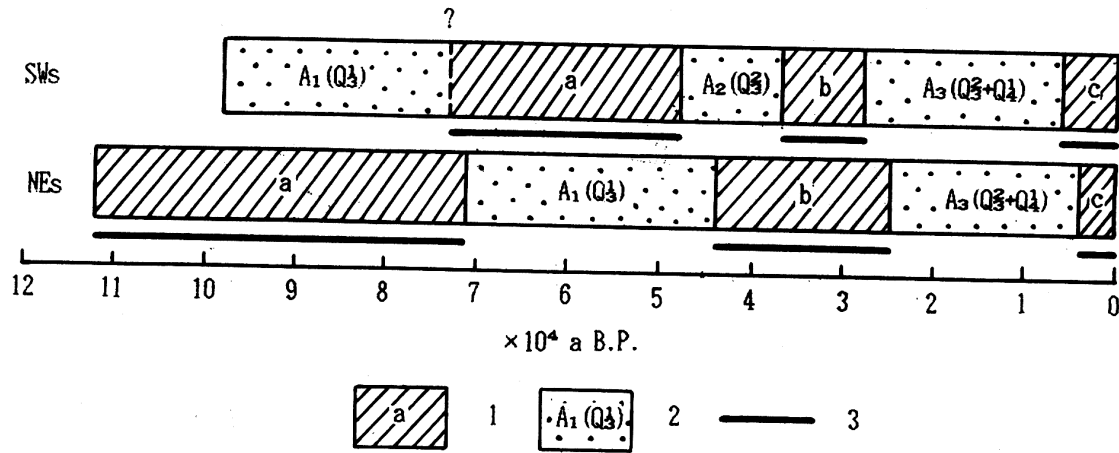


FIG. 9. Comparison of micro-physiographic stages for both segments, showing the difference prior to 36800 a B.P. and the consistence since 36800 a B.P.. (1) Erosional stage, (2) aggradational stage and (3) active period of faulting.

absence of the aggradation stage during which time the $A_2(Q_3^2)$ alluvial fan was accumulated. Although since 36800 a B.P. the same aggradational and erosional phases affected the fault zone, differences in the early physiographic history of the two segments led to the present-day laid the foundation of variations in their geomorphology.

REASON FOR VARIATIONS IN TECTONIC GEOMORPHOLOGY

Rates of Fault Displacement and Fluvial Downcutting

Vertical fault displacement rates

In Figure 10, the late-Quaternary fault scarp height reflects the apparent vertical fault displacement \bar{D}_a . The vertical distance between the fault scarp base and

the unconformity surface a, must be added to the cumulative vertical fault displacement D_a , in order to give the true accumulated vertical fault displacement for the SWs, i.e.,

$$D_a = \bar{D}_a + D_{a'-b'}$$

and for the Nes

$$D_a = \bar{D}_a + D_{a'-c'}$$

$D_{a'-b'}$ of the SWs can be approximated to the near-fault Q_3^2 deposit thickness, which was measured to be 5 m at Houzhikou (Fig. 4a). At the same sit, the fault scarp height was measured to be 20 m (Fig. 3a). For the SWs, since 73200 aB.P. (initiation of erosional microphysiographic stage a), the faulting rate is estimated to be $V_F = 0.34$ mm/a.

Table 4. Late-Quaternary micro-physiographic stages of both the segments.

fault segment	Time period (a B.P.)	Micro-physiographic stage characteristics
SWs (on the base of Fig. 6a)	98000-73200	Aggradational stage: Fault was inactive and $A_1 (Q_3^1)$ was deposited
	73200-48300	Erosional stage: Fault was active and $T_5 (Q_3^1)$ was formed and offset.
	48300-36800	Aggradational stage: Fault was inactive $A_1 (Q_3^2)$ deposited
	36800-27600	Erosional stage: fault was active and $T_4 (Q_3^2)$ and $T_3 (Q_3^2)$ were formed and offset.
	27600-5600	Aggradational stage: Fault was inactive and $A_3 (Q_3^2 + Q_4^1)$ was deposited.
	Since 5600	Erosional stage: Fault was active and $T_1 (Q_4^1)$ was formed and offset.
NEs (on the base of Figs. 5b, 6b and 7)	111500-70800	Erosional stage: Faulting was active, ancient lake was receded and erosional surface(a) was formed and offset.
	70800-43700	Aggradational stage: Faulting was inactive and $A_1 (Q_3^1)$ was deposited.
	43700-25000	Erosional stage: faulting was active, and erosional surface(b) was formed and offset.
	25000-3900	Aggradational stage: Fault was inactive and $A_3 (Q_3^2 + Q_4^1)$ was deposited.
	since 3900	Erosional stage: fault was active, and erosional surface(c) was formed and offset.

For the NEs, D_{a-c} is taken as the vertical distance between the fault scarp base and the surface of the Q_{1+2} lacustrine deposits, which is measured to be 85 m at Shipen (Fig. 2b). At the same site, the fault scarp height was measured to be 25 m (Fig. 3a). Since 111500 a B.P. (initiation of erosional micro-physiographic stage a), the faulting rate is estimated to be $V_F = 0.99 \text{ mm/a}$.

Fluvial downcutting rates

Based on near-fault maximum incision depths that were measured to be 30-35 m at Houzhikou for the SWs and 24m at Majiayao for the NEs, the fluvial downcutting rates can be estimated to be $V_D = 0.41-0.48 \text{ mm/a}$ and $V_D = 0.22 \text{ mm/a}$, respectively. The rates of faulting and downcutting are shown in Table 5.

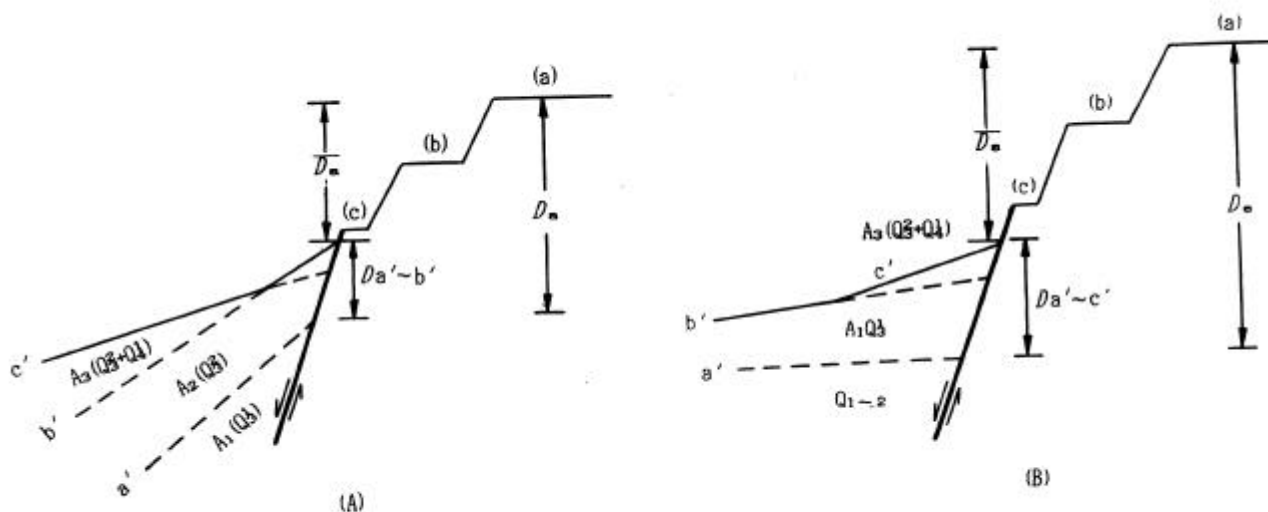


FIG. 10. Determination of the true accumulated vertical fault displacement, which is equal to the apparent vertical fault displacement plus a vertical distance between the fault scarp base and the unconformity surface a', for the SWs(A) and the NEs(B). (a), (b) and (c) represent erosional surfaces or terrace treads and a' b' and c' unconformity surfaces; Q_{1+2} Lacustrine deposits; and $A_1 (Q_3^1)$, $A_2 (Q_3^2)$, $A_3 (Q_3^2 + Q_4^1)$ alluvial fans. For explanatory notes of D_a , \bar{D}_a , $D_{a'-b'}$, and $D_{a'-c'}$ see the text.

Geomorphological effects

During the Late Quaternary, the SWs was characterised by a rate of downcutting higher than that of faulting ($V_F < V_D$) (Table 5). As the fault movement produced smaller cumulative displacement, river power sufficed to overcome the channel gradient difference caused by the faulting and the reaches of the streams on the upthrown block had smaller K values (Table 2).

Intensive stream erosion excavated passages on the piedmont slope to transport deposits. Meanwhile, faulting produced upwarping of this part of the piedmont slope, forming the alluvial fans inset into older ones.

In contrast, the Nes dominated with a rate of faulting higher than that of downcutting ($V_F > V_D$). Under conditions of larger cumulative displacement, river power overcame the difference of channel gradient produced by the faulting, and the reaches of the streams on the upthrow block had larger K values (Table 2). Rapid fault movement downwarped the near-fault side of the piedmont slope and the younger

alluvium was deposited, producing younger alluvial fans overlapping onto older ones.

Fault Behaviour

In addition to slip rate, other parameters of late-Quaternary fault behaviour including the interval between faulting events and the displacement during each event play an important role in the contrast between segments in their geomorphology. Numerous field observations show an average displacement per event of 3.1 m for the Nes but only 0.9 m for the SWs, indicating that the Nes has a faulting activity level greater than the SWs. On the basis of the duration of fault movement of the individual segments during the late-Quaternary (Fig. 9) and the cumulative displacement (Table 5), the average recurrence interval can be estimated to be 1800 a for the SWs and 1000 a for the Nes (Table 6). Consequently, both segments express significantly different fault behaviour. For the SWs, there is a small displacement per event and a short average recurrence interval, while for the Nes, it is opposite to the above.

Table 5. Rates of faulting and downcutting.

Fault Segment	Accumulated displacement (m)	Depth of dissection by stream (m)	Duration for calculating rate (a B.P)	Faulting rate V_F (mm/a)	Fluvial downcutting rate V_D (mm/a)	Comparitive relation
SWs	25	30-35	73200	.34	.41-.48	$V_F < V_D$
Nes	110	24	111500	.99	.22	$V_F > V_D$

Table 6. Data of fault behaviour.

Fault Segment	Average displacement per event (m)	Cumulative displacement (m)	Number of faulting events*	Total duration of fault movement (a)	Average recurrence interval** (a)
SWs	3.1	110	35	63300	1800
NEs	0.9	25	39	39700	1000

* Number of faulting events is obtained by dividing average displacement per event into the cumulative displacement.

** Average recurrence interval is obtained by dividing number of faulting events into the total duration of fault movement.

Segment Boundary: the Liyu-Dawangcun Overlapping faults

Overlapping faults and the intrabasin high

Geometrically, the boundary between the SWs and the NEs is characterized by faults overlapping along a length of 4.6 km from Liyu to Dawangcun. As shown in Figure 11a, the overlapping faults consists of an inside fault F_i and an outside fault F_o , which have a maximum separation of 1.35 km at the eastern tip near Dawangcun, but converge with the SWs at the western end near Liyu.

An area overlapped by faults where basement rocks are eroded is known as an intrabasin high (Anders and Schlische, 1994). The intrabasin high within the Liyu-Dawangcun fault overlap zone is exposed bedrock, geomorphologically becoming mountains with an elevation of 1240-1380 m. In the western part of the intrabasin high, there is an uplifted A_2 (Q_3^2) alluvial fan with a 25 m thick loessal soil, while in the east of the intrabasin high, there is a pediment that has a slope of 9.72° and a 4-8 m thick loessal soil cover, and a few 15-70 m high inselbergs.

Implications in fault segmentation: displacement deficit

The SWs has a vertical fault displacement of at least 25 m west of Liyu, while the overlapping faults have a cumulative displacement on F_o and F_i of only

20 m (I-I' and II-II' in Figure 11). The fact that the displacement on the main fault segment is not equal to the sum of the displacement on the branch faults indicates that a displacement deficit occurred on the overlapping faults. Moreover, as described above, the intrabasin high and the pediment on the basin side nearby the overlapping faults obviously result from incomplete basin depression produced by the displacement deficit. Consequently, the Liyu-Dawangcun overlapping fault zone represents a persistent segment boundary during the late-Quaternary time for the DYFZ.

CONCLUSIONS

1) Based on the late-Quaternary fault scarp heights and their alongstriking distribution pattern, the DYFZ can be divided into two discrete segments, the SWs and the NEs, each of these segments is characterized by fault scarp high reduction from the centre towards both its ends. Moreover, the fault scarps on the NEs are much higher than on the SWs.

2) As far as geomorphological indices that indicate mountain front tectonic geomorphology are concerned, there is a larger difference in K values but a smaller difference in S values and V_f values between both segments, indicating that both mountain front segments are principally controlled by faulting, especially with a greater faulting level on the NEs than on the SWs.

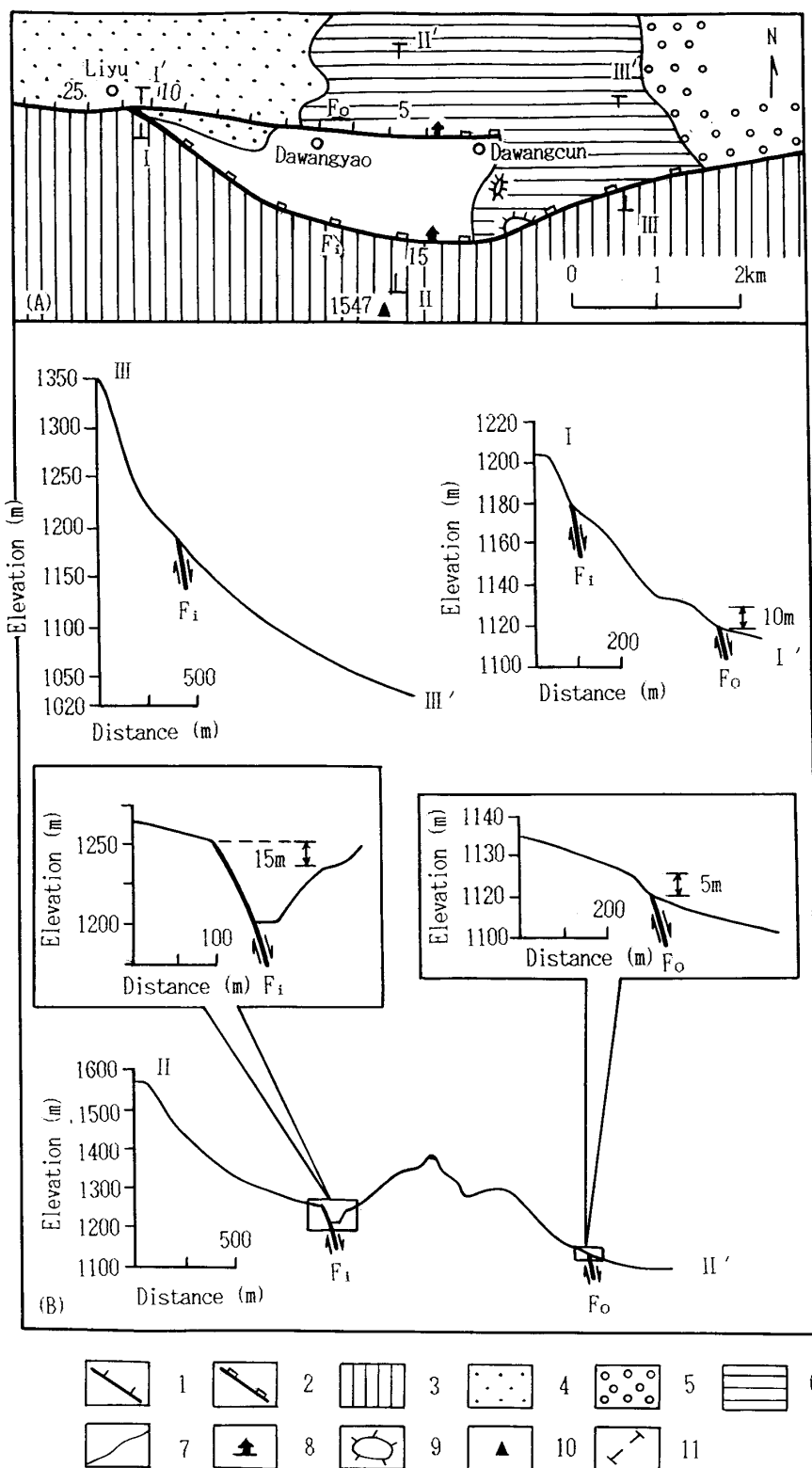


FIG. 11. Map of tectonic geomorphology of the Liyu-Dawangcun overlapping faults, showing geometry, displacement deficit, and characteristic landforms indicating displacement deficit. (A) Plan view; (B) Cross-sections. (1) Fault in loessal soil (numbers represent height, in meters), (2) Fault scarp in basement rocks (Numbers represent height, in metres), (3) Mountains 4) A₂ (Q₃²) alluvial fan, (5) A₃ (Q₃² + Q₄¹) alluvial fan, (6) pediment, (7) geomorphological unit boundary, (8) extensional direction, (9) inselberg, (10) summit (number represents elevation, in meters), (11) topographic profile and number. Fi ; inside fault, Fo; outside fault.

3) On the SWs piedmont slope, an upwarping occurred on the near-fault side of the $A_2(Q_3^2)$ alluvial fans, with the younger $A_3(Q_3^2 + Q_4^1)$ alluvial fans inset into the older $A_2(Q_3^2)$ alluvial fans; while for the NEs piedmont slope, a downwarping occurred on the near-fault side of the $A_1(Q_3^1)$ alluvial fans, with the younger $A_3(Q_3^2 + Q_4^1)$ alluvial fans overlapping onto the older $A_1(Q_3^1)$ alluvial fans.

4) Before 36800 a B.P., the NEs underwent stages of erosion-aggradation-erosion, while in contrast, the SWs underwent aggradation-erosion-aggradation. The different micro-physiographic stage history during the early phase of the Late-Quaternary has laid the foundation for the observed variations in tectonic geomorphology.

5) During the late-Quaternary, the SWs was characterised by a lower faulting rate (0.34 mm/a) relative to the fluvial downcutting rate (0.41-0.48 mm/a), with 0.9 m of average displacement per event and 1000 a average recurrence interval, while the NEs was characterised by a higher faulting rate (0.99 mm/a) relative to the fluvial downcutting rate (0.22 mm/a), with 3.1 m average displacement per event and an average recurrence interval of 1800 a. The boundary between the two segments is characterised by a fault overlap zone, along which a fault displacement deficit has occurred. Therefore, fault behaviour and the distribution of overlapping faults are conjointly responsible for the variations in geomorphology of the DYFZ.

ACKNOWLEDGMENTS

We thank the National Natural Science Foundation of China for support under Contract Numbers 49571011 and 49171011. We also thank Professor Ji Fengjie for thermoluminescence ages, and Professors Han Mukang and Wang Yipeng for suggestions. Specially, we thank Ms Justine Kemp, Research School of Earth Sciences, Australian National University, Mr Mehrooz Aspandiar and Mrs Judy Papps CRC LEME, Department of Geology,

Australian National University for editing the final manuscript.

REFERENCES

- Anders, M. H. and Schlische, R.W., 1994. Overlapping faults, intrabasin highs, and the growth of normal faults: *Journal of Geology*, **102**, 165-180.
- Bull, W.B. and McFadden, L.D., 1977, Tectonic geomorphology north and south of Garlock fault, California, in Doehring, D.O., Ed., *Geomorphology in Arid Regions*: Binghamton: State Uni. N.Y., 115-138.
- Chen Wenji, Li Daming, Dai Tongmo, Pu Zhiping, Liu Ruoxin, Li Qi, Shun Jingzhong, Wang Xin, Jager, E., Hurford, A.J., and Pfeifer, H.R., 1992, The K-Ar age and excess Ar of Quaternary basalt in Datong, In: Liu Ruoxin ed., *The Age and Geochemistry of Cenozoic Volcanic Rock in China*, Beijing: Seismological Press, 81-92 (in Chinese).
- Cheng Shaoping, Ynag Guizhi and Feng Jingjiang, 1991a, Attempts of weathering-rind thickness datings in the basalt area, northern North China: *ACTA Geographica Sinica*, **46(2)**, 242-251 (in Chinese with English abstract).
- Cheng Shaoping, Ynag Guizhi and Yang Zhe, 1991b, Longitudinal stream-profiles as indicators for geometric segmentation of the Langshan-Huangbaisi fault zone, Northwest Beijing: *Seismology and Geology*, **13(4)**, 300-309.
- Crone, A.J. and Heller, K.M., 1991, Segmentation and the coseismic behaviour of Basin and Range normal faults: examples from east-central Idaho and southwestern Montana, U.S.A.: *Journal of Structural Geology*, **13**, 151-164.
- Deng Qidong, Yonekuar Nobuyuki, Xu Xiwei, Yasuhiro Suzuke, Wang Cunyu, Takeuchi Akira, Su Zongzheng, Wang Yipeng, 1994, Study on the late Quaternary kinematics of the northern piedmont fault of the Liuleng mountain: *Seismology and Geology*, **16(4)**, 330-343 (in Chinese with English abstract).
- Hack, J.T., 1973, Stream profile analysis and stream-gradient index: *J. Res. USGS*, **1**, 421-429.
- Li Huhou, and Sun Jianzhong, 1984, Study on eras of Datong volcanic activities by thermoluminescence dating: *Scientia Sinica (Series B)*, **27**, 1069-1080.
- Mandl, G., 1988, *Mechanics of Tectonic Faulting: Models and basic concepts*: Amsterdam, Elsevier Science Publishers B.V., 407 p.
- Stewart, I.S. and Hancock, P.L., 1991, Scales of structural heterogeneity within neotectonic normal fault zones in the Aegean region: *Journal of Structural Geology*, **13**, 191-204.
- Wallace, R.E., 1978, Geometry and rates of change of fault-generated range fronts, north-central Nevada: *Journ. Res. USGS*, **6**, 637-650.
- Xia Zhengkai, 1992, Underwater loess and paleoclimate, *ACTA Geographica Sinica*: **47**, 58-65 (in Chinese with English abstract).
- Xu Xiwei, Ma Xingyuan, Deng Qidong and others, 1996, Neotectonics, paleoseismology and ground fissures of the Shanxi (Fen-Wei) Rift System, China: 30th International Geological Congress Field Trip Guide T₃₁₄, Beijing: Geological Publishing House, 152 p.